PERGAMON

Journal of Structural Geology 22 (2000) 1455–1468

JOURNAL OF STRUCTURAL GEOLOGY

www.elsevier.nl/locate/jstrugeo

Localization of layer-parallel faults in San Rafael swell, Utah and other monoclinal folds

Kaj M. Johnson*, Arvid M. Johnson

M. King Hubbert Structural Geology Laboratory, Department of Earth and Atmospheric Sciences, Purdue University, West Lafayette, IN 47907, USA

Received 29 July 1999; accepted 5 April 2000

Abstract

The subdivision of sedimentary rock layers by the formation of layer-parallel faults in a developing fold can be explained by a combination of intralayer weaknesses and internal layer-parallel shear stresses generated by bending. An analysis of stress equilibrium of layer-parallel shear stresses and fiber normal stresses indicates that the maximum shear stress increases with the square of the thickness and the layer-parallel derivative of curvature, termed here coil, evaluated at middepth of the bed. The maximum shear stress is at middepth in the layer, so a laminated bed, as it bends, will tend to fault at middepth along pre-existing layer-parallel weaknesses and thereby subdivide the single mechanical layer into two mechanical layers of half the original thickness. Using the method of computation of coil outlined here, we are able to show that the coil predicts the location and sense of shear of layer-parallel faults in several field examples. The method illustrates how a few careful field measurements of layer geometry can provide valuable information about conditions of folding. © 2000 Published by Elsevier Science Ltd.

1. Introduction

In the course of a study of the monocline along the eastern margin of the San Rafael swell, Utah, we noticed in some places, within the central limb of the fold, that massive sandstone beds contain many layer-parallel faults whereas in other places they do not. Preliminary observations indicated that the presence of the layer-parallel faults within the central limb correlates with the tightness of the fold. Where the fold is quite broad—radius of curvature of 760 m—there are few layer-parallel faults. Where the fold is quite tight—radius of curvature of 40 m—layer-parallel faults are abundant.

Other researchers have observed slip surfaces parallel to bedding in steep limbs of folds, so our observations are not unique. Cook and Stearns (1975) mapped faults parallel to cross-bedding in a monoclinal fold at Dinosaur National Monument, Utah. Aytuna (1984) and Pfaff (1986) mapped layer-parallel faults in kink bands ranging in width from a few meters to a few hundred meters in the central Appalachians. Bevan (1984) noted the existence of slip planes parallel to bedding within the steep limb of the Isle of Wight monocline, England. Jackson and Pollard (1990) mapped bedding-parallel faults within the dipping limbs of a monoclinal folds that formed around the periphery of several laccolithic intrusions in the Henry Mountains, Utah.

Studies relevant to the analyses presented here have been conducted by various authors. Ramsay (1967) suggested that the amount of layer-parallel slip in an idealized fold is proportional to the tangent of the limb dip. Chapple and Spang (1974) showed that the shear strain rate increases with dip of the bedding during folding of an anisotropic, linearly viscous layer. Koch et al. (1981) explained why monoclinal flexures form around the periphery of some laccolithic intrusions and showed that the monoclinal flexing is a result of layer-parallel slip at the periphery. Cooke et

* Corresponding author. Fax: +1-765-496-1210.
E-mail address: kaj@expert.cc.purdue.edu (K.M. Johnson).

0191-8141/00/$ - see front matter © 2000 Published by Elsevier Science Ltd.
PII: S0191-8141(00)00046-8

al. (1998) used a Boundary Element Method to show that layer-parallel faults will be localized within the limb of a monocline. The analysis suggests that frictional slip would initiate above the centerline and within the steep limb of the folded layer.

Layer-parallel faulting is important to understanding folding because it allows a stiff, single, thick mechanical layer to subdivide into a flexible multilayer composed of thinner mechanical units. Couples et al. (1998) proposed that bedding-parallel slip surfaces were activated during bending of strata at Rattlesnake Mountain anticline, Wyoming. Their observations suggest that slip surfaces were progressively activated as bending proceeded, creating more and more slip surfaces and a greater number of mechanical units. Furthermore, Couples et al. (1998) demonstrated with an experimental model and numerical model that, during bending, slip occurs first on the middle interface, and then in later stages of bending the slip is distributed to the outer layers.

The purpose of this paper is to propose a simple theoretical explanation, using elementary beam theory, for the formation of layer-parallel faults such as those described by Couples et al. (1998) as well as several examples that we have observed. We also show how to make field measurements of the parameters that control the faulting.

2. Field examples of layer subdivision

2.1. Spotted Wolf section of San Rafael swell

The San Rafael swell, located in central Utah, is an asymmetric, domical uplift stretching about 50 km east and west and 120 km north and south. Beds over the center and on the west edge of the uplift dip gently westward. A magnificent monoclinal fold, with a central limb dipping eastward, dominates the eastern edge of the swell. The central limb is characterized morphologically by dramatic flat-irons of Navajo Sandstone (Fig. 1). The Spotted Wolf section of the monocline extends 10 km from Spotted Wolf Canyon (at Interstate 70) in the north to Iron Wash in the south.

The Spotted Wolf section was chosen for study because the central limb has a wide range of dip angles and radii of curvature within the same rock units. The radius of curvature of the synclinal hinge ranges from 760 m, near I-70, to 40 m near mid-length of the section. At both ends of the Spotted Wolf section, the fold hinges are wide open, the monocline is broad, and dips are relatively shallow, 30° or less (Fig. 1a). In the middle part of the section, the fold hinges are much tighter, the monocline is much narrower and the beds within the central limb dip much more steeply and are locally overturned (Fig. 1b).

Small faults in the form of deformation bands[1] formed parallel to cross-bedding in the Navajo Sandstone in places along the Spotted Wolf section (Fig. 2; Johnson, 2000). The Navajo Sandstone is a massive, cross-bedded sandstone. Bedding planes are difficult to locate, in part because beds can be as thick as several tens of meters, but large low-angle cross-beds provide layering of the Navajo. At the same locations where faults formed parallel to cross-bedding in the Navajo Sandstone, faults did not form parallel to cross-bedding in the more thinly bedded, cross-stratified Entrada Sandstone.

The frequency and occurrence of faults parallel to

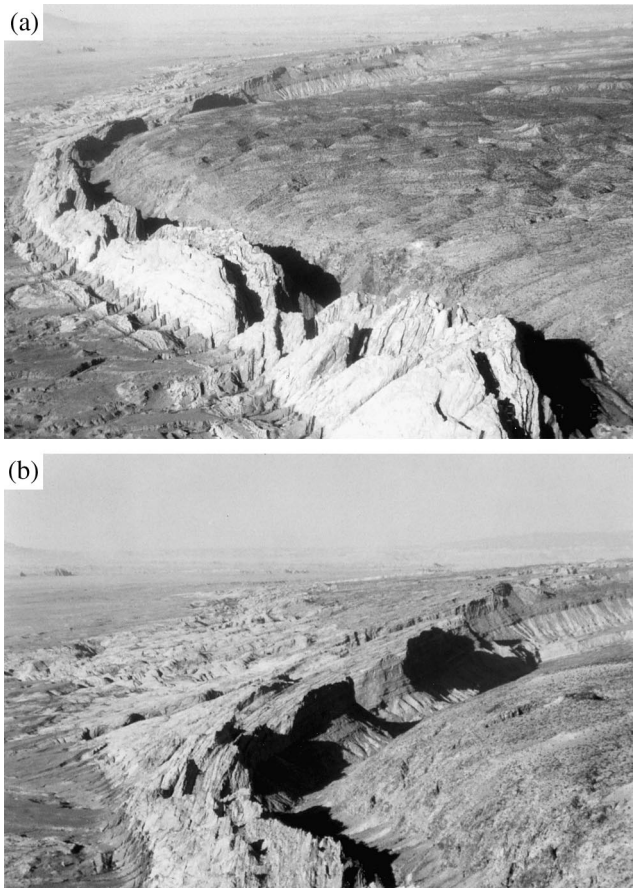

Fig. 1. (a) Arial view of San Rafael swell, Spotted Wolf section. I-70 is out of view to the right. White face of flat-irons is Navajo Sandstone. (b) Arial view of southern end of Spotted Wolf section. Sudden change in dip is evident with beds dipping steeply in the bottom of the picture and shallowly in the top.

[1] Deformation bands are thin, tabular bodies of highly localized cataclasis in porous sandstones. They have been studied in detail by several investigators (Aydin, 1977, 1978; Aydin and Johnson, 1978, 1983; Jamison and Stearns, 1982; Underhill and Woodcock, 1987; Cruikshank et al., 1991; Zhao and Johnson, 1991; Antonelli et al., 1994).

Fig. 2. Cross-bedding-parallel faults in the Navajo Sandstone. White highlighted cross-bedded surfaces are deformation bands that accommodate small amounts (not measurable) of slip. Lens cap in lower left for scale.

bedding or low-angle cross-bedding vary from place to place along the Spotted Wolf section and appear to correlate with tightness of the synclinal hinge and with thickness of bedding in sandstone units. The frequency of cross-bed-parallel faults, where radius of curvature of the synclinal hinge is of the order of 50 m, is much higher than where the radius of curvature of the synclinal hinge is of the order of 1000 m. For example, small cross-bed-parallel faults are scarce in large roadcuts where I-70 provides nearly perfect exposures in the Navajo Sandstone at the northern end of the Spotted Wolf section. In contrast, they are abundant where the fold is tight in steeply dipping Navajo beds near the synclinal hinge.

2.2. Shikellamy fold

The spacing of layer-parallel faults was documented in a railroad cut in the Shikellamy fold (Fig. 3), a monoclinal fold in the Sherman Creek Member of the Catskill Formation, along the northwest bank of the Susquehanna River at Northumberland, Pennsylvania (Aytuna, 1984). The central limb of the Shikellamy fold is about 150 m long.

The Shikellamy fold is characterized by layer-parallel faults that are sparse in the outer limbs and numerous in the central limb. The spacing of layer-parallel faults ranges from 0.25 to 0.7 m within the central limb. In contrast, the spacing is 2–4 m in the southern outer limb and 25 m in the northern outer limb of the fold. As noted by Aytuna (1984), the sense of shear parallel to bedding, as viewed in Fig. 3, was right-lateral for faults in the steep central limb and the outer northern limb and left-lateral for faults in southern outer limb.

2.3. Amity Hall fold

Pfaff (1986) studied monoclinal folds in interbedded mudstone and siltstone in central Pennsylvania. One of these folds (Fig. 4) is exposed in a roadcut near Amity Hall, along highway 22/322 along the Juniata River, about 35 km northwest of Harrisburg, Pennsylvania. The rocks are part of the Devonian Trimmers Rock and Brallier formations. The fold is shown via a sketch of traces of fractures; bedding surfaces were not mapped. Thus the spacing of the lines indicates the spacing of fractures. The sketch shows that the central limb of the fold, which is about 2 m long, is more thoroughly delaminated than the two outer limbs

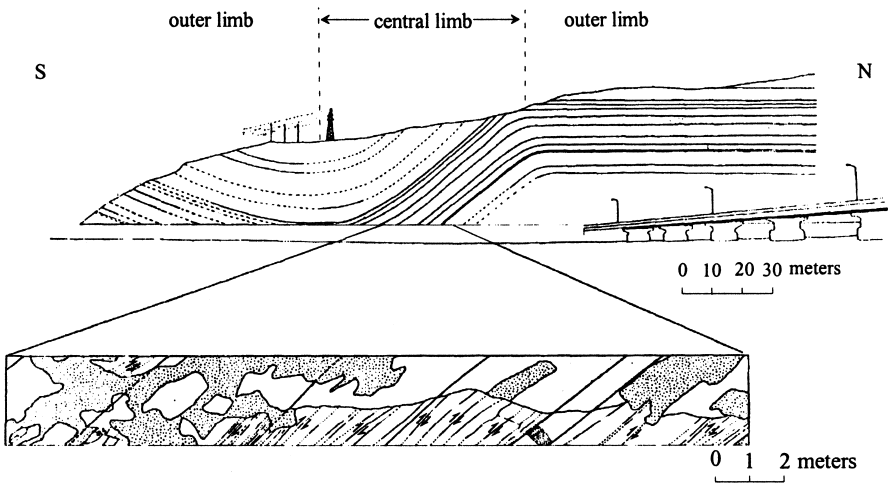

Fig. 3. Shikellamy fold, Pennsylvania. Faults are mapped in detail in the lower picture. Right-lateral bedding-parallel faults are localized within the central limb.

(Fig. 4a). The number of fractures at least doubles in the central limb.

The extra fractures in the central limb extend only as far as the fold hinges, as shown in a detailed sketch (Fig. 4b) of the synclinal hinge marked with a rectangle in Fig. 4(a). The sketch shows several layer-parallel faults that accommodated about 1–2 cm of right-lateral slip and terminated near the hinges of the fold. The (mechanical) hinges separate right-lateral from left-lateral shearing on the upper and lower surfaces of the layer.

3. Theoretical analysis of layer subdivision

3.1. The problems

The three monoclinal folds all have layer-parallel faults within the central limbs. In two of the three field examples—the narrow, 2 m wide, Amity Hall monoclinal fold and the 150 m wide, Shikellamy fold—the layer-parallel faults are much more closely spaced within the short central limbs than in the long outer limbs on both sides of the folds. We mapped the entire width of the central limb of the Amity Hall fold, and in this case we could see that the layer-parallel faults extend essentially from hinge to hinge. In the much larger—1500 m width—monocline on the east side of San Rafael swell, we could map cross-bed-parallel faults in sandstone only near the synclinal hinge of the central limb.

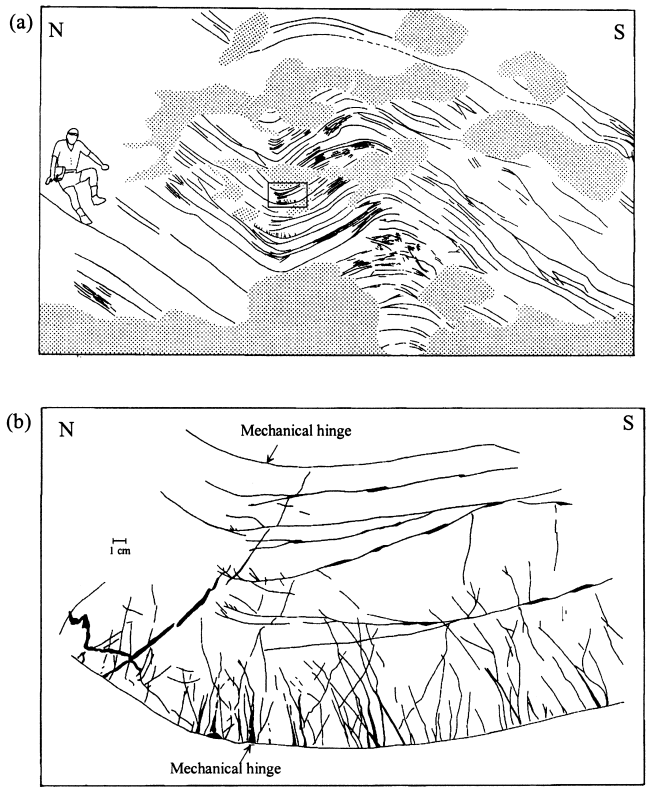

Fig. 4. (from Pfaff, 1986) (a) Map of traces of fractures in Amity Hall fold. Localization of bedding-parallel fractures in steep limb (Mapped by A.M. Johnson). (b) Detail map of hinge marked with a box in (a). (Mapped by V. Pfaff).

Based on these field observations, we choose to ask the following questions about the subdivision of sedimentary rocks by formation of layer-parallel faults: How do layer-parallel faults form along pre-existing layer-parallel weakness in a bent layer? Why did faults form parallel to cross-bedding in the massive Navajo Sandstone but not in the more thinly bedded Entrada Sandstone? And, why did cross-bedding-parallel faults form in the Navajo Sandstone near the tight synclinal hinge where the radius of curvature is 40 m but not near the broad synclinal hinge where the radius of curvature is 760 m?

3.2. Shear stress within a bent layer

The shear stress responsible for formation of layer-parallel faults can be generated within a bent layer by a change in curvature with position in the layer. We will derive a relationship between shear stress and curvature using elementary beam and plate theory (e.g. Marin and Sauer, 1954; Timoshenko and Goodier, 1961).

In beam and plate theory, the bending of a layer is described solely in terms of a linear distribution of normal stress and normal strain parallel to the layer. For the positive curvature shown in Fig. 5(a), the layer-parallel normal stresses are compressive at the top, tensile at the bottom, and zero at middepth (Fig. 5b). These stresses are known as the fiber stresses. For a thin beam it is assumed that they have the linear form,

$$\sigma_f = B\kappa n \tag{1a}$$

in which B is an elasticity modulus,

$$B = \frac{E}{(1-\nu^2)}. \tag{1b}$$

E is Young's modulus, ν is Poisson's ratio, κ is curvature at middepth of the layer, and n is the radial distance from middepth. Thus the fiber stresses are proportional to the curvature.

The shear stress distribution within the layer depends on the boundary conditions as well as the change in fiber stresses along the layer. The top and bottom boundaries at the layer contacts (Fig. 5b) are subjected to a shear stress, τ_{cont}. This stress derives from the mechanical interaction between the layer and its surroundings. For example, if slip between layers is left-lateral, the layers are subjected to left-lateral shear

at contacts, τ_{cont}. If the layers slip freely past each other, τ_{cont} is zero. The element of the layer (Fig. 5b) is also subjected to shear stresses, $\tau(n)$, along its sides.

In order to derive an expression for the shear stress distribution through an element (Fig. 5b) we select a piece of the element (Fig. 5c) that includes the upper surface of the layer and a thickness δn of the element. Acting on each side of the piece are the linear fiber stress distributions and the unknown shear stress distributions, $\tau(n)$. Acting on the top is the shear stress, τ_{cont}, and on the bottom is $\tau(n_0)$. The fiber stresses change across the piece.

The fiber stresses at the left-hand end of the piece of the element are given by Eq. (1a), whereas the fiber stresses at the right-hand side of the piece are,

$$\sigma_f + \frac{\partial \sigma_f}{\partial s}\delta s = B\left[\kappa + \frac{d\kappa}{ds}\delta s\right]n. \tag{1c}$$

As indicated in Eq. (1c), the change in curvature, $\frac{d\kappa}{ds}\delta s$, across the element results in a change in the fiber stresses, $\frac{\partial \sigma_f}{\partial s}\delta s$, across the element; it is this change in curvature and fiber stresses that generates the shear within the layer.

We define $\tau(n_0)$ as the shear stress generated at the bottom of the piece of the element. Its relation to the change of fiber stresses, and curvature, is obtained by summing forces equal to zero in the horizontal direction,

$$[\tau_{cont} - \tau(n_0)]\delta s \frac{d\kappa}{ds}\delta s B\int_{n_0}^{T/2} n dn = 0. \tag{2a}$$

Thus the shear stress along the base of the piece of the element is,

$$\tau(n_0) = \tau_{cont}\frac{d\kappa}{ds}B\int_{n_0}^{T/2} n dn$$

$$= \tau_{cont}\frac{d\kappa}{ds}(B/2)[(T/2)^2 - n_0^2] \tag{2b}$$

in which the sign ($\pm$) of τ_{cont} is determined from the slip direction of the beds (τ_{cont} is positive for right lateral slip). Eq. (2b) also gives the shear stress, $\tau(n_0)$, on the vertical sides of the piece, adjacent to the base (Fig. 5c).

Eq. (2b) indicates that the relation between shear stress, $\tau(n_0)$, and distance from middepth, n_0, is parabolic (Fig. 5b). Thus the shear stress on the base of the tiny element increases from the boundary value, τ_{cont}, at the top of the layer ($n_0 = T/2$) to its maximum value, τ_{mid}, at middepth ($n_0 = 0$) in the layer:

$$\tau_{mid} = \tau_{cont}\frac{d\kappa}{ds}\frac{BT^2}{8}. \tag{2c}$$

3.3. Geometric interpretation of curvature and coil

We will use Eq. (2c) to understand why layer-paral-

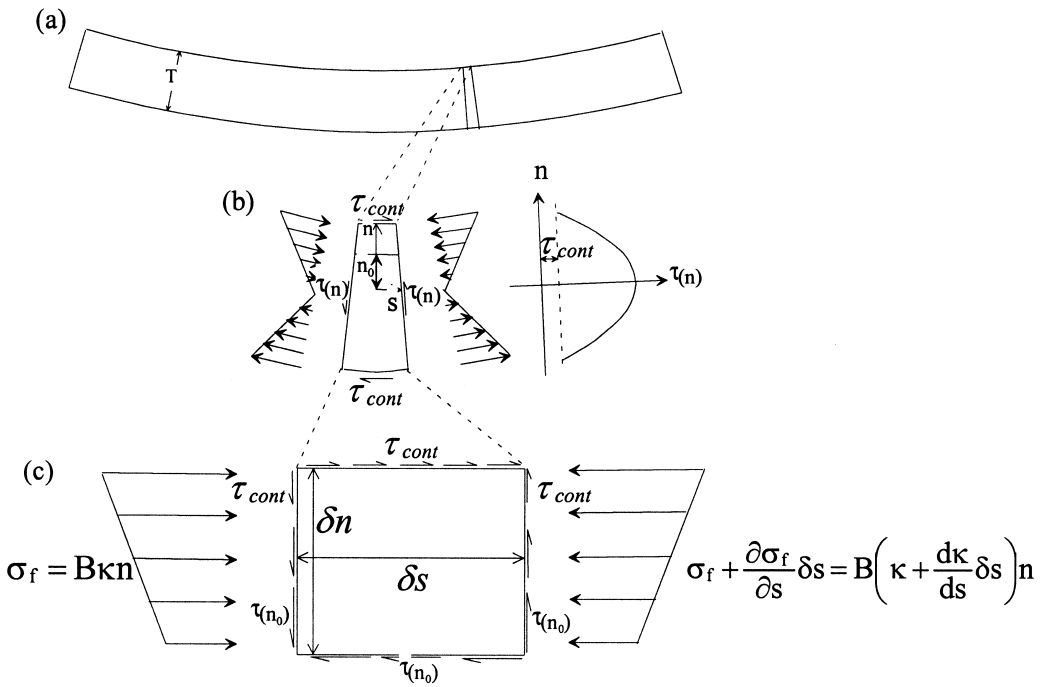

Fig. 5. (a) Bent beam. (b) Element of beam showing fiber stress distribution, layer-normal shear stress, $\tau(n)$, distribution, and contact stress, τ_{cont}, on top and bottom surfaces. (c) Small piece of element with fiber stresses, σ_f, and layer normal shear stresses.

lel faults form, but first we must discuss the derivative of curvature with respect to arc length, $d\kappa/ds$, which we term coil. Coil can be interpreted geometrically using curvature, $\kappa = d\theta/ds$, where $\tan\theta$ is the slope of the layer. Curvature can be visualized geometrically with the radius of curvature, $\rho = 1/\kappa$. The radius of curvature is the radius of the circle constructed at a point along a curve with the same curvature and tangent as the curve. The derivative of curvature with respect to distance, s, or coil, at a point is

$$\frac{d\kappa}{ds} = \frac{d^2\theta}{ds^2}. \tag{3a}$$

The coil can be visualized with two nearby radii of curvature. Fig. 6a shows a curve with an open bend that becomes progressively tighter with distance along the curve. The open bend has a radius of curvature ρ_1 at point 1, and the tight bend a distance δs away has a much smaller radius of curvature ρ_3 at point 3. In terms of radius of curvature, the coil given by Eq. (3a) at the midpoint, 2, becomes

$$\left[\frac{d^2\theta}{ds^2}\right]_2 = \left[\frac{d}{ds}\left(\frac{1}{\rho}\right)\right]_2 \approx \frac{\frac{1}{\rho_3} - \frac{1}{\rho_1}}{s_3 - s_1} = \frac{-1}{\rho_3\rho_1}\left(\frac{\rho_3 - \rho_1}{s_3 - s_1}\right). \tag{3b}$$

An extreme value is obtained from a circle (Fig. 6b). It has zero coil everywhere because

$$\frac{1}{\rho_2} - \frac{1}{\rho_1} = 0.$$

The coil of a straight line is also zero because a straight line is the limit of a circle with an infinite radius of curvature.

3.4. How layers subdivide by layer-parallel faulting

Eq. (2c) suggests an explanation for the experimental and numerical results by Couples et al. (1998) that slip occurs first on the middle interface in a bending multilayer. Our analysis shows that change in bending with position along the layer generates layer-parallel

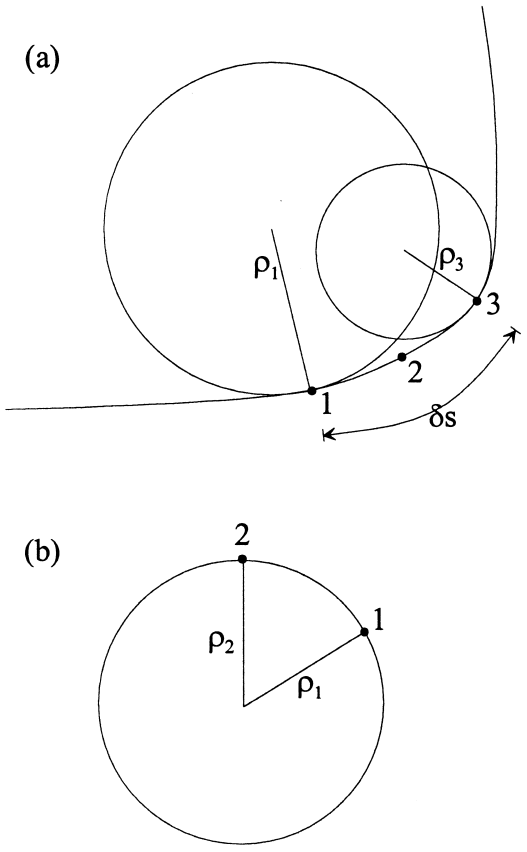

Fig. 6. (a) Coil at point 2 can be visualized with change in radius of curvature from point 3 to 1. (b) The coil along a circle is zero since $\rho_1 = \rho_2$ for any two points 1 and 2 on a circle.

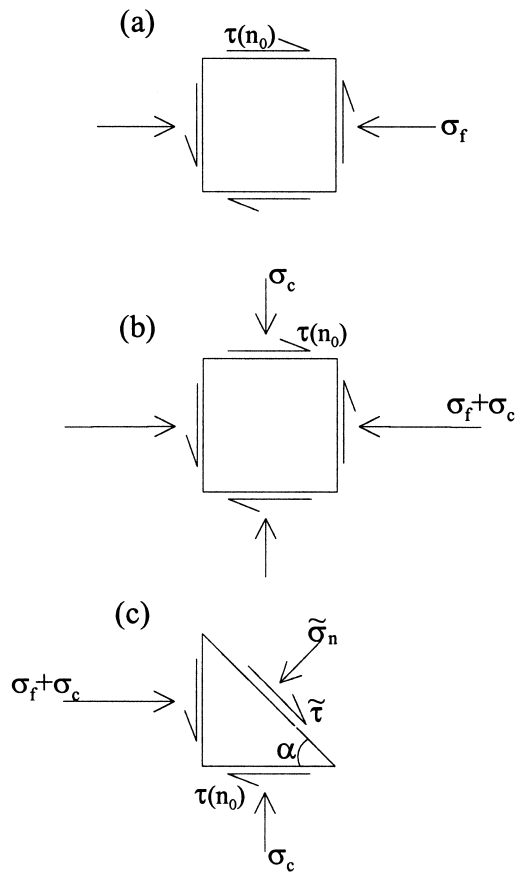

Fig. 7. Stress state within a bent beam. (a) Bending induces a layer-parallel fiber stress σ_f and shear stress $\tau(n_0)$. (b) Included with the bending stresses is a confining pressure, σ_c. (c) Tractions acting on a surface inclined α degrees to the fiber stresses and layer.

shear stress and that the position of the maximum value is at middepth in a layer. The analysis, though, is incomplete without consideration of the effect of the normal stress acting on the slip surface.

To make the analysis complete, we assume that failure occurs according the Coulomb failure criterion, thus slip occurs along an interface when

$$\tilde{\tau} = C + \mu\tilde{\sigma}_n \tag{4a}$$

where $\tilde{\tau}$ and $\tilde{\sigma}_n$ are the shear and normal tractions resolved on the interface, C is cohesion, and μ is the coefficient of internal friction. We analyze the stress state shown in Fig. 7(a) and determine the planes of failure in the case of a homogeneous layer. The stress state is determined at every point within the layer with the shear and fiber stresses (Fig. 7a). Pure bending does not generate a normal stress perpendicular to the layer according to elementary beam theory, but we include an arbitrary confining stress, σ_c (Fig. 7b). The shear and normal tractions (Fig. 7c) on a surface inclined at an angle α to the direction of fiber stresses are:

$$\tilde{\tau} = \tau(n_0)\cos(2\alpha) - \frac{\sigma_f}{2}\sin(2\alpha) \tag{4b}$$

$$\tilde{\sigma}_n = \frac{(\sigma_f + 2\sigma_c)}{2}\frac{\sigma_f}{2}\cos(2\alpha) - \tau(n_0)\sin(2\alpha) \tag{4c}$$

at any point in the layer.

We calculate the stress ratio $\tilde{\tau}/\tilde{\sigma}_n$ using 4 and replacing $\tau(n_0)$ with τ_{mid} in order to determine if failure will occur at middepth of a bent layer. Fig. 8(a) is a plot of the stress ratio $\tilde{\tau}/\tilde{\sigma}_n$ at middepth of the layer where $\sigma_f = 0$. In Fig. 8(a), τ_{mid} is determined with Eq. (2c) using $\tau_{cont} = 0$ and reasonable values for B (5.05×10^{10} N/m^2), dκ/ds (2.5×10^{-4} m^{-2}), and T (100 m). If we assume a cohesionless rock with a typical friction coefficient of 0.6 (Byerlee, 1978), then we can see in Fig. 8(a) that failure in an isotropic layer will occur on planes oriented at angles $\alpha = 15^\circ$ and 75°, where the stress ratio $\tilde{\tau}/\tilde{\sigma}_n$ equals the strength, 0.6. The stress ratio parallel to layering, at $\alpha = 0^\circ$, is lower than the

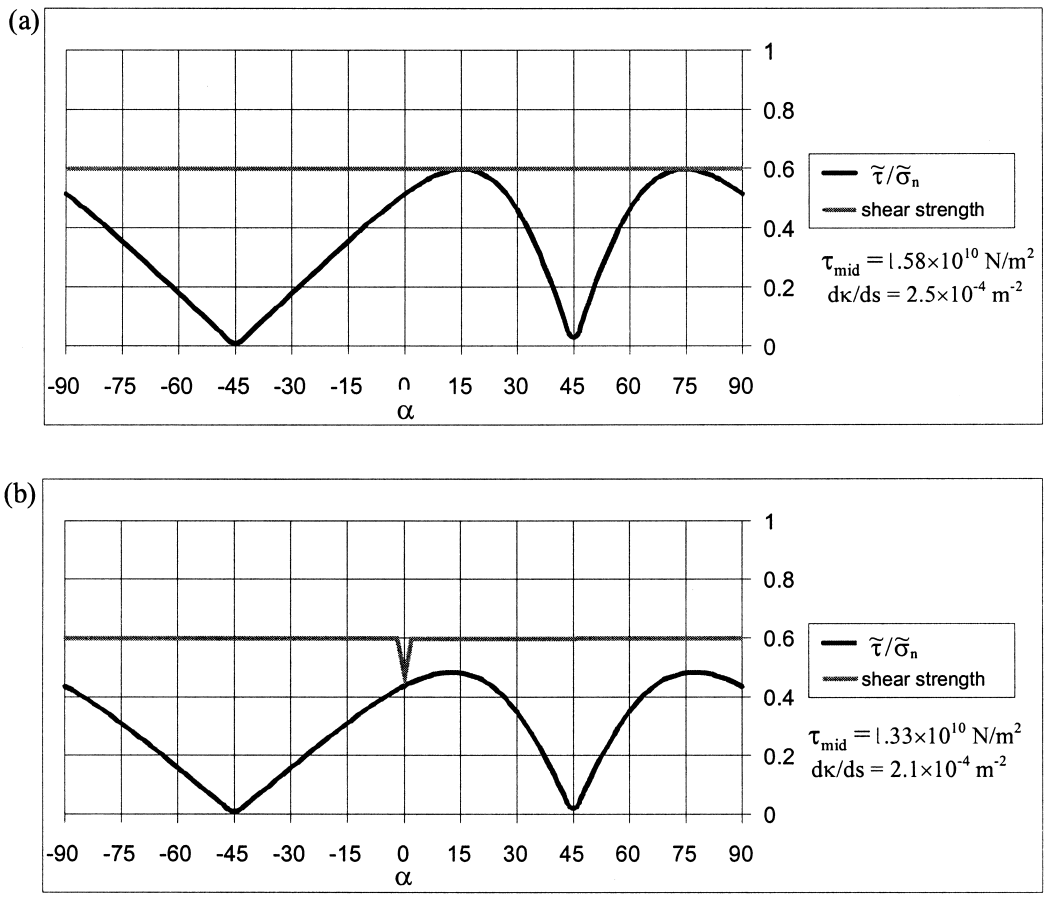

Fig. 8. Stress ratio $\tilde{\tau}/\tilde{\sigma}_n$ at middepth of a layer ($\sigma_f = 0$) on surfaces inclined α degrees to the layer. (a) Isotropic layer with layer-parallel shear stress at middepth is 1.58×10^{10} N/m^2. Failure occurs on planes oriented at $\alpha = 15^\circ$ and a $= 75^\circ$ where the stress ratio $\tilde{\tau}/\tilde{\sigma}_n$ equals the strength 0.6. (b) Anisotropic layer with layer-parallel planes of low strength. At a lower layer parallel shear stress of 1.33×10^{10} N/m^2, failure occurs on the layer-parallel weak surface.

strength, 0.6, so failure cannot occur parallel to layering.

If the layer is not isotropic, but rather contains preexisting bedding parallel planes ($\alpha = 0$) of lower strength (Fig. 8b), then at a lower $d\kappa/ds$ value (2.1×10^{-4} m^{-2}) the stress ratio $\tilde{\tau}/\tilde{\sigma}_n$ can equal the shear strength on the weak surfaces, before the ratio $\tilde{\tau}/\tilde{\sigma}_n$ equals failure at 0.6 in other directions (Fig. 8b). Thus failure will occur on the bedding-parallel weak surfaces at an earlier stage in bending of the rock, before the stress ratio $\tilde{\tau}/\tilde{\sigma}_n$ can become large enough for failure to occur on the planes oriented at angles $\alpha = 15^\circ$ and 75°. This is a reason sedimentary bedding with bedding-parallel laminations tends to form layer-parallel faults.

We have shown that, if a fault forms at middepth due to bending stresses (i.e. shear and fiber stresses), the fault will form along layer-parallel weaknesses, if they exist. We will now show that a layer-parallel fault will form at middepth of the layer before a layer-parallel fault forms at any other depth. At any point in the layer, when $\alpha = 0$, $\tilde{\tau} = \tau(n_0)$ and $\tilde{\sigma}_n = \sigma_c$. Thus at any point in the layer, it is the ratio of the layer-parallel shear stress and the layer-normal confining stress, $\tau(n_0)/\sigma_c$, that determines whether failure occurs along bedding-parallel weaknesses. But since σ_c is constant, it is $\tau(n_0)$ that determines whether a bedding-parallel fault forms. We showed in Eq. (2b) that $\tau(n_0)$ is maximum at middepth of the layer where the shear stress is τ_{mid} (Eq. 2c). Thus if the shear strength parallel to bedding planes is constant and lower than the shear strength in all other directions, the first place the stress ratio $\tau(n_0)/\sigma_c$ will equal the layer-parallel shear strength will be at middepth, and a layer-parallel fault will subdivide the layer at middepth.

3.5. Effect of contact strength between layers on layer-parallel faulting

If we suppose that the contact stress, τ_{cont}, is negligible, that is, we suppose that layers slip freely over one another, then Eq. (2c) indicates that the layer-parallel shear stress is proportional to the elasticity modulus, B, to the square of the thickness of the original layer, T^2, and to the coil, $d\kappa/ds$. Other things being equal, the stiffest, thickest layer in a stack of layers will tend to subdivide first as magnitude of the coil is increased. Suppose all the layers are of the same stiffness (same elastic modulus, B) but of different thicknesses, and suppose the layers are laminated with preexisting planes of weakness parallel to layering. As the layers are bent, the layer-parallel shear stresses will increase until the shear strength is first overcome at middepth of the thickest layer and the layer subdivides. If all the layers are of the same thickness but of different stiffnesses, then the stiffest layer will tend to subdivide first.

In either case, we now have two layers of thickness $T/2$. Each layer has a parabolic distribution of shear stress, but the maximum shear stress has been reduced by a factor of four. As the coil increases, the shear stress increases and each of these laminated layers, in turn, becomes subdivided. Now we have four layers of thickness $T/4$, and the layer originally of thickness T is a multi-layer.

In order to explain the effect of contact strength on the subdivision of layers we define the shear stress generated by the coil, $d\kappa/ds$, such that

$$\tau_{coil} = -\frac{d\kappa}{ds}\frac{BT^2}{8}. \tag{5a}$$

Eq. (2c) then can be written

$$\tau_{mid} = \tau_{cont} + \tau_{coil}. \tag{5b}$$

In this form we can visualize the effect of the contact stress, τ_{cont}, on intralayer stress at middepth, τ_{mid}. Whether the contact stress adds to or subtracts from the intralayer shear stress at middepth depends on the sense of interlayer slip. By definition, right-lateral shear stress is positive. Right-lateral slip, therefore, increases τ_{mid} when τ_{coil} is positive ($d\kappa/ds < 0$) and decreases τ_{mid} when τ_{coil} is negative ($d\kappa/ds > 0$).

3.6. Cross-bedding-parallel faults in Navajo Sandstone

It appears as though we can understand the abundance of cross-bedding-parallel faults in the Navajo Sandstone as compared to the lack of cross-bedding-parallel faults in the Entrada in terms of bedding thicknesses of these formations. The Entrada Sandstone contains many cross-bedded layers with thicknesses of a few meters. The Navajo Sandstone on the other hand, contains only a few beds with thicknesses of ~100 m, but has numerous cross-bedding surfaces. If contact stress is neglected, the middepth shear stress, τ_{mid}, is proportional to the square of the thickness and directly proportional to the coil, Eq. (2c). Assuming similar coils in the two rock units, the middepth shear stress in the massive Navajo Sandstone should be 400–10,000 times larger than the middepth shear stress in the beds of the Entrada Sandstone. Thus there is a much higher tendency for layer-parallel faulting in the Navajo than in the Entrada.

We must not ignore the fact that the cross-bedding surfaces are not bedding-parallel but are typically oriented at an angle $\alpha < \pm 20^\circ$ to the fiber stresses and the bedding planes. In Fig. 8(a and b) we can see that the stress ratio $\tilde{\tau}/\tilde{\sigma}_n$ is smaller at $\alpha = \pm 20^\circ$ than at $\alpha = 0^\circ$. However, the planes of weakness in the Navajo Sandstone clearly are restricted to large cross-beds and

not to bedding-parallel surfaces. Thus the faults tend to occur along the weak, cross-bedding surfaces rather than parallel to bedding.

3.7. Critical coil

For a layer-parallel fault to form, the coil at mid-depth must be large enough for the stress ratio $\tau_{mid}/\tilde{\sigma}_n$ to overcome the internal shear strength of the layering within the bed. Thus, there is a critical value for the layer-parallel shear stress, τ_{crit}, and therefore the coil, at which layer-parallel faults occur. This critical coil value is obtained from Eq. (2c) after substituting τ_{crit} for $\tau_{mid}\infty$:

$$\left(\frac{d\kappa}{ds}\right)_{crit} = \frac{8(\tau_{cont} - \tau_{crit})}{BT^2}. \quad (6a)$$

In dimensionless form, Eq. (6a) can be written as

$$\left(\frac{d\kappa}{ds}\right)^*_{crit} = \frac{\tau_{cont} - \tau_{crit}}{B} \quad (6b)$$

in which the nondimensional coil is

$$\left(\frac{d\kappa}{ds}\right)^*_{crit} = \left(\frac{d\kappa}{ds}\right)_{crit}\left(\frac{T^2}{8}\right). \quad (6c)$$

The coil and the thickness of the layer being bent are clearly the most important geometric parameters that we need to measure in order to understand why layer-parallel faults occur. These parameters combine to form the nondimensional coil, Eq. (6c), a quantity that we can compare from fold to fold at all scales.

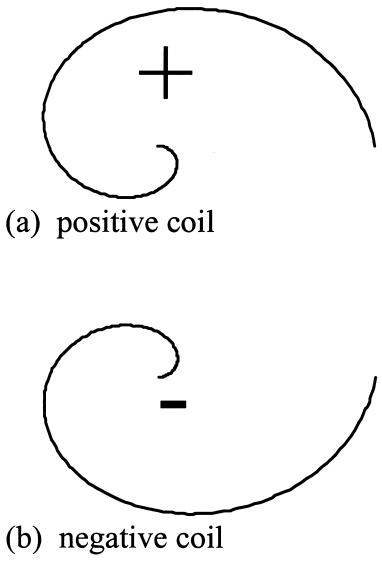

Fig. 9. Negative and positive coil. (a) Positive Archimedes' coil has positive coil at every point. (b) Negative Archimedes' spiral has negative coil at every point.

4. Measuring curvature and coil

4.1. Coil

We need to be able to determine the sign and magnitude of coil, $d\kappa/ds$, along folded layers in order to determine locations of high layer-parallel shear stress, and thus locations of layer-parallel faulting. The sign of the coil at a point is determined by Eq. (3b) and is illustrated with Archimedes' spirals in Fig. 9. One has positive coil and the other has negative coil at every point on the curve. While traversing a curve in a clockwise direction, if at a point the curvature changes from larger to smaller, the coil is negative, as is the case at every point on the negative spiral in Fig. 9(b). While traversing a curve in a counterclockwise direction, if at a point the curvature changes from smaller to larger, the coil is positive, as is the case at every point on the positive spiral in Fig. 9(a). In the example of Fig. 6(a), the coil is positive at point 2 since the curvature changes from smaller at point 1, to larger at point 3 as we traverse the curve in a counterclockwise direction.

4.2. Measurement of curvature and coil in the field

We will develop a method for calculating curvature and coil along a contact in a cylindrical fold using field measurements. The method requires five dip measurements along a line normal to the strike of the cylindrical fold, and the distances between pairs of these points, measured along the fold (Fig. 10). The curvature, $d\theta/ds$, is calculated at points (s_2,θ_2), (s_3,θ_3), and (s_4,θ_4), and then the coil is calculated at point (s_3,θ_3) with these $d\theta/ds$ values.

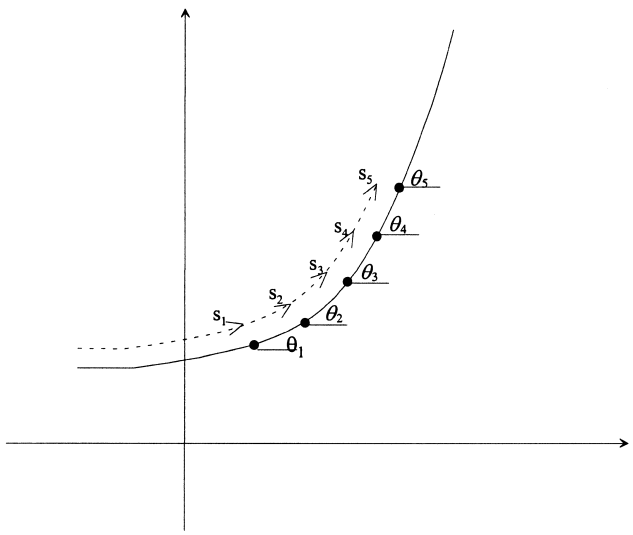

Fig. 10. Hypothetical profile of a fold and five points spaced unevenly along the fold. Coil can be approximated at (s_3,θ_3) with 7.

The method presented here (after Nakamura, 1996) allows for unequal spacing of the five points. We want to allow for uneven spacing of points because the field data may not be available everywhere on the fold. We first outline the procedure delineated in 7 before deriving the steps.

The curvature, $d\theta/ds$, is calculated at a point (s_i,θ_i) using the three points (s_{i-1}, θ_{i-1}), (s_i,θ_i), and (s_{i+1}, θ_{i+1}). The derivative, $d\theta/ds$, is assumed to have the form

$$\left(\frac{d\theta}{ds}\right)_i = a_i\theta_i + a_{i-1}\theta_{i-1} + a_{i+1}\theta_{i+1} \tag{7a}$$

in which the coefficients are the solution to the equations,

$$a_i + a_{i-1} + a_{i+1} = 0$$

$$0 + a_{i-1}\{s_{i-1} - s_i\} + a_{i+1}\{s_{i+1} - s_i\} = 1$$

$$0 + a_{i-1}\{s_{i-1} - s_i\}^2 + a_{i+1}\{s_{i+1} - s_i\}^2 = 0 \tag{7b}$$

or,

$$\begin{bmatrix} a_i \\ a_{i-1} \\ a_{1+1} \end{bmatrix} = \begin{bmatrix} \dfrac{(s_{i-1} - s_i)^2 - (s_{i+1} - s_i)^2}{(s_{i+1} - s_i)(s_{i-1} - s_i)(s_{i+1} - s_{i-1})} \\ \dfrac{s_{i+1} - s_i}{(s_{i-1} - s_i)(s_{i+1} - s_{i-1})} \\ \dfrac{-(s_{i-1} - s_i)}{(s_{i+1} - s_i)(s_{i+1} - s_{i-1})} \end{bmatrix}. \tag{7c}$$

The coil, $d^2\theta/ds^2$, is determined at (s_3,θ_3) using the curvature values calculated at (s_2,θ_2), (s_3,θ_3), and (s_4,θ_4). The coil is calculated as a derivative of first derivatives of the form:

$$\left(\frac{d^2\theta}{ds^2}\right)_3 = a_3\left(\frac{d\theta}{ds}\right)_3 + a_2\left(\frac{d\theta}{ds}\right)_2 + a_4\left(\frac{d\theta}{ds}\right)_4. \tag{7d}$$

Here the coefficients a_2, a_3, and a_4 are the same as in Eq. (7c) with $i = 3$ since the spacing is the same.

Now we will explain how 7 are derived. The method deals with unequally spaced points by expressing the functions $\theta(s)$ and $d\theta/ds$ in Eq. (7a) and Eq. (7d) as a Taylor expansion. This can be illustrated with Eq. (7a); Eq. (7d) is expanded in the same way.

Recognizing that a function, $\theta(s)$, can be written as a Taylor expansion about a point s_i,

$$\theta(s) = \sum_{n=0}^{\infty} \frac{\theta^{(n)}(s_i)(s - s_i)^n}{n!}$$

Eq. (7a) can be expressed:

$$\left.\frac{d\theta}{ds}\right|_i = a_i\theta(s_i) + a_{i-1}\left[\theta(s_i) + \theta'(s_i)\{s_{i-1} - s_i\} + \frac{\theta''(0)}{2!} \times \{s_{i-1} - s_i\}^2 + \frac{\theta'''(0)}{3!}\{s_{i-1} - s_i\}^3 + \cdots\right] + a_{i+1}\left[\theta(s_i) + \theta'(s_i)\{s_{i+1} - s_i\} + \frac{\theta''(0)}{2!} \times \{s_{i+1} - s_i\}^2 + \frac{\theta'''(0)}{3!}\{s_{i+1} - s_i\}^3 + \cdots\right]. \tag{8a}$$

After reorganizing terms and dropping third-order and higher terms,

$$\left.\frac{d\theta}{ds}\right|_i \approx \theta(s_i)[a_i + a_{i-1} + a_{i+1}] + \theta'(s_i)[a_{i-1}\{s_{i-1} - s_i\} + a_{i+1}\{s_{i+1} - s_i\}] + \frac{\theta''(s_i)}{2!}\left[a_{i-1}\{s_{i-1} - s_i\}^2 + a_{i+1}\{s_{i+1} - s_i\}^2\right]. \tag{8b}$$

To solve for the coefficients, we set the coefficients of $\theta(s_i)$, $\theta'(s_i)$, and $\theta''(s_i)$ in Eq. (8b) to 0, 1, 0, respectively:

$$a_i + a_{i-1} + a_{i+1} = 0$$

$$0 + a_{i-1}\{s_{i-1} - s_i\} + a_{i+1}\{s_{i+1} - s_i\} = 1$$

$$0 + a_{i-1}\{s_{i-1} - s_i\}^2 + a_{i+1}\{s_{i+1} - s_i\}^2 = 0. \tag{8c}$$

Thus we have derived equations equivalent to Eq. (7b).

The error of the solution can be estimated with the higher-order term that is not used to determine the coefficients, $\frac{\theta'''(0)}{3!}[a_{i-1}s_{i-1}^3 + a_{i+1}s_{i+1}^3]$. Because we neglect terms with third and higher derivatives, the result is a second-order approximation.

4.3. Distribution of coil illustrated on a structural profile

Dip angle, θ, and its first derivative, curvature, $d\theta/ds$, are familiar geometric quantities that we use to describe folds. For example, curvature has been used to determine the location of joint formation in folded beds (e.g. Fischer and Wilkerson, 2000). Although coil, the second derivative of slope angle, $d^2\theta/ds^2$, is less familiar, it relates to the subdivision of layered rocks, so it is a quantity with which we should become familiar.

A strike view of the Palisades monocline, Grand Canyon, Colorado, constructed by Reches (1978) can be used to demonstrate coil on a structural profile. The Palisades monocline is a branch of the East Kai-

bab monocline near the confluence of the Colorado and Little Colorado rivers. The canyon of Palisades Creek is about 1200 m deep and offers an unusual opportunity to examine the actual geometry within a monocline, based on first-hand observations. The upper part of the canyon was mapped by a combination of photogrammetry and field observation, and the lower part was mapped with plane-table methods, so the map, and the derivative strike view (Fig. 11) are highly accurate. The result is a clear view of a monocline, from a near-vertical fault zone in Precambrian, basement rocks to the Permian, Coconino Sandstone and Kaibab Limestone at the canyon rim (Fig. 11).

We can describe the shapes of the contacts between formations in terms of coil. Fig. 11a displays normalized coil, expressed in units of 10^{-2}, calculated at locations along four contacts. The average thickness of the formations in the monocline is about 200 m, so we use a thickness of $T = 200$ m to obtain the normalized coil. The shaded parts of Fig. 11a show locations of large coil. The arrows show sense of shear. Of course, coil does not completely determine whether layer-parallel faults form, because formation of such faults depends also on the thickness of the bed and the strength in shear along layering of the rock. We can, however, determine directly from these measurements where in a fold thick beds are likely and unlikely to be divided by layer-parallel faults.

The largest values for coil in the Palisades monocline occur adjacent to sharp hinges (Fig. 11a). The upper and lower contacts of the Bright Angel Shale (Cambrian) have slightly different forms. The lower contact is adjacent to the basement fault and the beds are steep to overturned there. The contact has sharp synclinal and anticlinal hinges. Fig. 11a shows that the coil is large adjacent to both hinges. The contact between the top of the Bright Angle Shale and the bottom of the Muav Limestone (Cambrian) is about 100 m above the end of the basement fault. It has a sharp synclinal hinge and an open anticlinal hinge. Fig. 11a shows that the coil is large only adjacent to the sharp synclinal hinge.

The contact between the top of the Temple Butte Limestone (Cambrian) and the bottom of the Redwall Limestone (Mississippian) has a distinct synclinal hinge but no anticlinal hinge; it is probably outside the view to the right. The coil is small and highly localized near a contraction fault in the contact at the base of the Redwall. The top of the Redwall is broadly folded and does not have sharp hinges. The coil is small in the top of the Redwall and it decreases rapidly and the fold broadens upward, away from the fault.

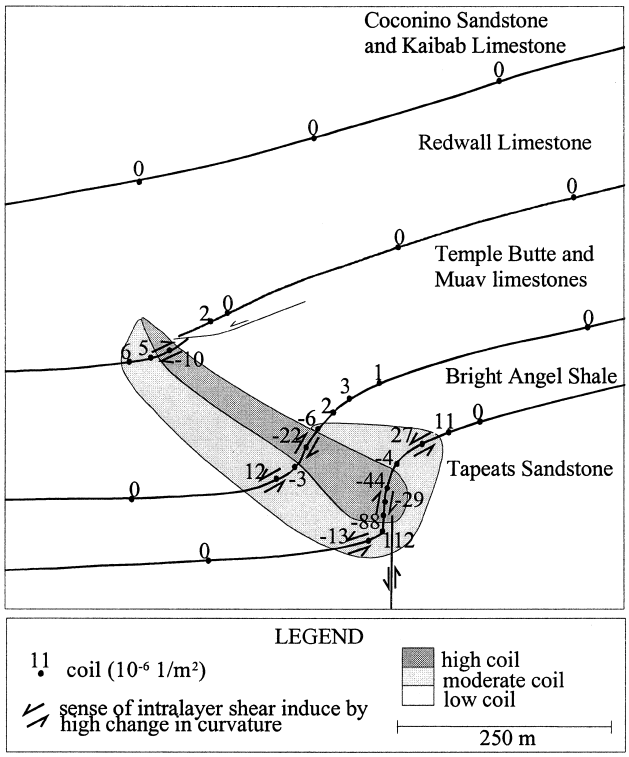

Fig. 11. Accurate composite cross-section of the Palisades monocline. Coil was calculated at each of the indicated locations. The largest coil at each interface is located adjacent to the sharp hinges.

5. Location of layer-parallel faults in field examples

5.1. Amity Hall monoclinal fold

The shape of the Amity Hall fold (Fig. 4) is characteristic of a monoclinal kink band (Reches and Johnson, 1976). It has sharp hinges, with radii of curvature of about 0.6 m, and straight limbs, with larger radii of curvature of 3–4 m. Layer-parallel faults in the fold are in both the short central and long outer limbs. There is a high concentration of layer-parallel faults adjacent to the sharp hinges within the central limb of the fold (Fig. 4a).

In this example we know the spacing of faults and we can measure coil, so we should be able to understand why the layer-parallel faults are distributed as they are. We measured the coil at ten locations along layer-parallel faults in the fold. The measurements of normalized coil are plotted in Fig. 12. They show that the locations of the high concentration of faults in the central limb adjacent to the hinges correspond with the locations of largest magnitude of normalized coil of -1.6 and $+1.6$ near the anticlinal hinge and -1.9 near the synclinal hinge.

The high normalized coil on both sides of the hinges suggests that we might expect a concentration of layer-parallel faults near the hinge in

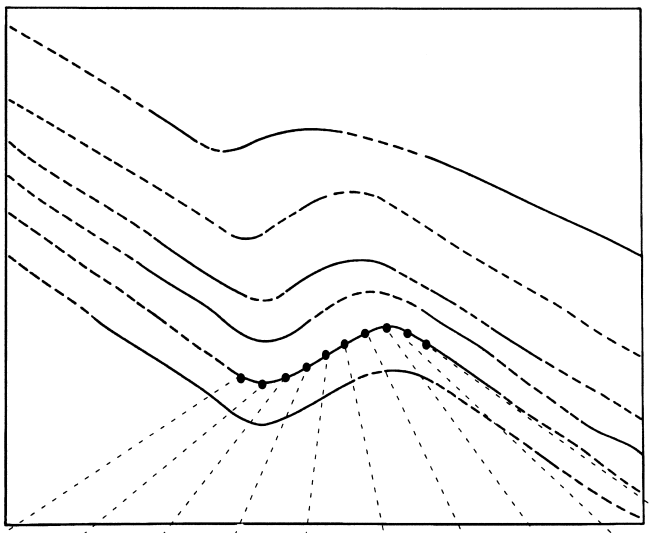

ρ (m)	1.3	0.7	1.7	12.8	-3.6	-3.4	-2.7	-0.6	-3.3	-3.2
normalized coil ($\times 10^{-2}$)	---	-0.7	-1.9	-0.1	-0.4	-0.1	-1.6	0.3	1.6	---

Fig. 12. Calculations of radius of curvature and coil at ten points along a bedding contact in the Amity Hall fold. The largest coil is located adjacent to the sharp hinges.

both the outer limbs and the inner limb. We observe that the faults are concentrated, though, only on the central limb.

The lack of faults on the outer limbs can be understood if the Amity Hall fold did indeed form as a kink band and we consider the effect of the contact stress, τ_{cont}. To obtain the kink band form, it is necessary that there be frictional or cohesive contact strength[2] between layers according to Honea and Johnson (1976) and Reches and Johnson (1976). This is so because, for an isolated kink band to form (without a train of folds), it is necessary that the bending moment be zero at the edge of the band. They have shown that, for this to occur, the contact stress, τ_{cont}, Eq. (2b), must be some non-zero critical value equal to the adhesive strength between adjacent layers. Consider now Eq. (2c) and, in the case of our view of the Amity Hall Fold, a positive value for τ_{cont} applied to the layers. Then the effect of τ_{cont} on the middepth layer-parallel shear stresses, τ_{mid}, is to increase τ_{mid} in the central limb where the coil is negative (τ_{coil} is positive), and decrease τ_{mid} on the outer limbs where the coil is positive (τ_{coil} is negative). It is therefore likely that an effect of the contact stress was to reduce the intralayer shear stresses on the outer limbs to the extent of preventing layer-parallel faults from forming there, as observed in the field example.

The pattern of layer-parallel faults in the Amity Hall fold brings up two additional issues that are beyond the scope of this paper. The simplest issue is that the layer-parallel faults grow during fold development so that they cause the fold to change shape as it grows. In effect, a single thick layer locally changes to a multilayer laminate as the fold grows. This must cause the fold form to evolve. A corollary is that the measurements of coil represent only the last stages of growth of the folds as we see them. Another issue is that this paper concerns only the shear stresses generated by bending, whereas kink folds form under conditions of maximum compression subparallel to layering in the outer limbs (Reches and Johnson, 1976). Therefore, one should expect that the maximum compression will contribute to the layer-parallel shear on dipping limbs.

5.2. San Rafael swell monocline

The question of why cross-bedding faults are abundant in the Navajo Sandstone at San Rafael swell near the tight fold hinges, whereas they are scarce near the broad fold hinges, can be addressed with the result in Eq. (2c) and Eq. (3b). First, we assume that the shear stress is solely a result of bending. Then Eq. (2c)

[2] Pfaff (1986) and Johnson and Pfaff (1989) have shown that nonlinear resistance to slip, say of a power-law form, is sufficient to cause kink-like folds to form. The resistance need not be so highly nonlinear as strength.

shows that the shear stresses at middepth of the layer, when $\tau_{cont}=0$, are proportional to the coil, $d\kappa/ds$, of the bent layer. The coil near the tight synclinal hinge, where cross-bed-parallel faults were observed, is larger than near the synclinal hinge of the broader part of the fold, where cross-bed-parallel faults were not observed.

The radius of curvature was measured in several places within the Carmel Formation, which overlies the Navajo Sandstone, and in the Entrada Sandstone, which overlies the Carmel. At a location where the synclinal hinge of the Entrada Sandstone is tight (Fig. 13), the radius of curvature in the hinge is $\rho=40$ m ($\kappa=25\times10^{-3}$ m^{-1}). At a location within the Carmel Formation where the synclinal hinge is broad, the radius of curvature is $\rho=760$ m ($\kappa=1.3\times10^{-3}$ m^{-1}). The difference is more than an order of magnitude.

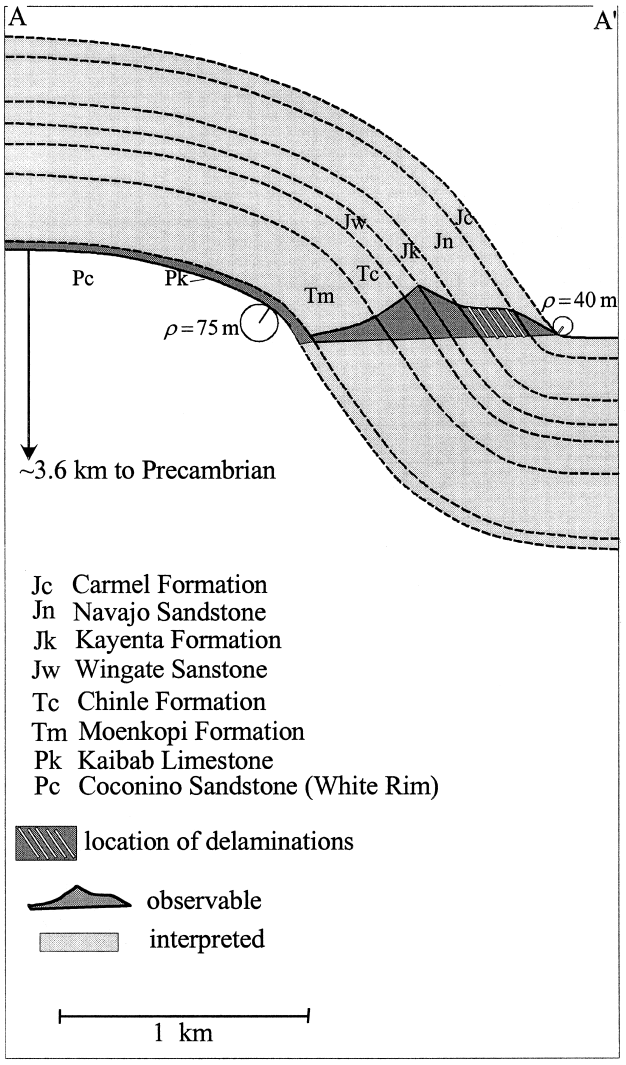

Fig. 13. Cross-section of steep section of San Rafael Swell monocline. Radius of curvature of the synclinal hinge was measured in the field near the bottom of the Entrada Sandstone. Radius of curvature in the upper anticlinal hinge was measured from a topographic map. Dark shaded section is exposed in the field. The lighter shaded section is inferred.

We can roughly estimate the coil if we assume the curvature is zero on the central limb of the fold and both of the measured hinges are the same distance, Δs (measured in meters), from the location of zero curvature, then the coil adjacent to the broad hinge is

$$\frac{d\kappa}{ds}=\frac{\frac{1}{760}-0}{\Delta s}=\frac{1}{760\Delta s}\ (\mathrm{m}^{-2})$$

and the coil adjacent to the tight hinge is

$$\frac{d\kappa}{ds}\approx\frac{\frac{1}{40}-0}{\Delta s}=\frac{1}{40\Delta s}\ (\mathrm{m}^{-2}).$$

Therefore the coil is nearly 20 times larger at the location with the tighter hinge. Assuming the bed thickness at both locations is the same (200 m for Navajo Sandstone), the middepth shear stress within the Navajo at the location with the tighter hinge would have been nearly 20 times the middepth shear stress at the other location (Eq. 2c). Furthermore, if the spacing of the two measurements of curvature is an arc distance of Δs = 500 m, the normalized coil in the tighter hinge is about 0.5 whereas that in the open hinge is about 0.026. Thus it seems clear that the concentration of cross-bedding-parallel faults near the synclinal hinge of the Spotted Wolf section of the San Rafael swell is associated with the magnitudes of the coil in those locations.

6. Discussion and conclusions

Analysis of elementary beam theory shows that layer-parallel shear stresses within a bent layer are maximal at middepth of the layer and increase with coil. Furthermore, the high layer-parallel shear stresses along pre-existing surfaces of weakness causes layer-parallel faulting. Thus, as a fold progresses and the coil increases, the strata will progressively subdivide into thinner and thinner mechanical layers until the generated shear stress is no longer large enough to cause slippage.

We presented several examples where layer-parallel faulting has occurred in monoclinal folds and showed that coil is maximal in these locations. In this sense, coil predicts sites of layer-parallel faults.

The concept of coil can be understood in terms of familiar geometric concepts. The curvature, κ, is defined as the change in slope angle, θ, with a change in arc distance, ds, along a line. The coil is the change in curvature with a change in arc distance along the

line. The coil at a point can thus be estimated with measurements of dip angles along the fold.

In general one is unable to make field measurements of dip angle spaced at uniform arc distances for calculating coil. Thus we present a method for unequally-spaced measurements. One can calculate coil along a line of curvature if one measures dips at five points equally or unequally spaced along the line of curvature and the distance between each point, measured along the arc-length of the bed.

Acknowledgements

We would like to thank Raymond Fletcher and Michele Cooke for their helpful reviews. Their comments greatly improved the manuscript. This research was made possible by the generous efforts of Kaj's field assistant and wife, Cyndi Johnson, and financial support for field work by the Donald Levandowski memorial award and the Cedric J. Newby award, Department of Earth and Atmospheric Sciences, Purdue. The remainder of the field expenses were paid by Department of Energy grant DE-FG02-98ER14886, supervised by Nick Woodward of DOE. We appreciate the support of these organizations.

References

Antonelli, M.A., Aydin, A., Pollard, D.D., 1994. Microstructure of deformation bands in porous sandstone at Arches National Park, Utah. Journal of Structural Geology 16, 941–959.

Aydin, A., 1977. Faulting in sandstone. Ph.D. dissertation, Stanford University.

Aydin, A., 1978. Small faults formed as deformation bands in sandstone. Pure and Applied Geophysics 116, 913–930.

Aydin, A., Johnson, A.M., 1978. Development of faults as zones of deformation bands and as slip surfaces in sandstone. Pure and Applied Geophysics 116, 931–942.

Aydin, A., Johnson, A.M., 1983. Analysis of faulting in porous sandstones. Journal of Structural Geology 5, 19–31.

Aytuna, S., 1984. Forms of large folds in the central Appalachians, Pennsylvania. Ph.D. dissertation, University of Cincinnati.

Bevan, T.G., 1984. Tectonic evolution of the Isle of Wight: a Cenozoic stress history based on mesofractures. Proceedings of the Geologists Association of London 96 (3), 227–235.

Byerlee, J.D., 1978. Friction of rocks. Pure and Applied Geophysics 116, 615–626.

Chapple, W.M., Spang, J.H., 1974. Significance of layer-parallel slip during folding of layered sedimentary rocks. Geological Society of America Bulletin 85, 1523–1534.

Cook, A.C., Stearns, D.W., 1975. Mechanisms of sandstone deformation: a study of the drape folded Weber Sandstone in Dinosaur National Monument, Colorado and Utah. In: Bolyard, D.W. (Ed.), Symposium on Deep Drilling Frontiers of the Central Rocky Mountains. Rocky Mountain Association of Geologists, Denver, pp. 21–32.

Cooke, M.L., Mollema, P., Pollard, D.D., Aydin, A., 1998. Interlayer slip and joint localization in East Kaibab Monocline, Utah: Field evidence and results from numerical modeling. In: Cosgrove, J. (Ed.), Forced (Drape) Folds and Associated Fractures. Geological Society of London, Special Publication, No. 169.

Couples, G.D., Lewis, H., Tanner, P.W.G., 1998. Strain partitioning during flexural-slip folding. In: Coward, M.P., Daltaban, T.S., Johnson, H. (Eds.), Structural Geology in Reservoir Characterization. Geological Society of London, Special Publications 127, London, pp. 149–165.

Cruikshank, K.M., Zhao, G., Johnson, A.M., 1991. Duplex structures connecting fault segments in Entrada Sandstone. Journal of Structural Geology 13, 1185–1196.

Fischer, M.P., Wilkerson, M.S., 2000. Predicting the orientation of joints from fold shape: Results of pseudo-three-dimensional modeling and curvature analysis. Geology 28, 15–18.

Honea, E., Johnson, A.M., 1976. Development of sinusoidal and kink folds in multilayers confined by rigid boundaries. Tectonophysics 30, 197–239.

Jackson, M.D., Pollard, D.D., 1990. Flexure and faulting of sedimentary host rocks during growth of igneous domes, Henry Mountains, Utah. Journal of Structural Geology 12, 185–206.

Jamison, W.R., Stearns, D.W., 1982. Tectonic deformation of Wingate Sandstone, Colorado National Monument. American Association of Petroleum Geologists Bulletin 66, 2584–2608.

Johnson, A.M., Pfaff, V.F., 1989. Parallel, similar and constrained folds. Engineering Geology 27, 115–180.

Johnson, K.M., 2000. Methods of Structural Analysis of the Spotted Wolf Section of the San Rafael Monocline, Utah. MS thesis, Purdue University.

Koch, F.G., Johnson, A.M., Pollard, D.D., 1981. Monoclinal bending of strata over laccolithic intrusions. Tectonophysics 74, T21–T31.

Marin, J., Sauer, J.A., 1954. Strength of Materials. MacMillan Co, NY.

Nakamura, S., 1996. Numerical Analysis and Graphic Visualization with Matlab. Prentice-Hall, Inc, New Jersey.

Pfaff, V.J., 1986. On forms of folds. PhD dissertation, University of Cincinnati.

Ramsay, J.G., 1967. Folding and Fracturing of Rocks. McGraw-Hill, New York.

Reches, Z., 1978. Development of monoclines: Part I. Structure of the Palisades Creek branch of the East Kaibab monocline, Grand Canyon, Arizona. In: Mathews, V. (Ed.), Laramide Folding Associated with Basement Block Faulting in the Western United States. Geological Society of America Memoir, USA, p. 151.

Reches, Z., Johnson, A.M., 1976. Asymmetric folding and monoclinal kinking. Tectonophysics 35, 295–334.

Timoshenko, S., Goodier, J.N., 1961. Theory of Elasticity. McGraw-Hill Book Co, NY.

Underhill, J.R., Woodcock, N.H., 1987. Faulting mechanisms in high-porosity sandstones; New Red Sandstone, Arran, Scotland. In: Jones, M.E., Preston, R.M.F. (Eds.), Deformation of Sediments and Sedimentary Rocks. Geological Society Special Publication, 29, pp. 91–105.

Zhao, G., Johnson, A.M., 1991. Sequential and virtual formation of conjugate sets of faults. Journal of Structural Geology 13, 887–895.